

Article

# A Decision Support System for Melanoma Diagnosis from Dermoscopic Images

Maria Rizzi \*  and Cataldo Guaragnella 

Dipartimento di Ingegneria Elettrica e dell'Informazione (DEI), Politecnico di Bari, 70125 Bari, Italy;  
cataldo.guaragnella@poliba.it

\* Correspondence: maria.rizzi@poliba.it

**Abstract:** Innovative technologies in dermatology allow for the early screening of skin cancer, which results in a reduction in the mortality rate and surgical treatments. The diagnosis of melanoma is complex not only because of the number of different lesions but because of the high similarity amongst skin lesions of different nature; hence, human vision and physician experience still play a major role. The adoption of automatic systems would aid clinical assessment and make the diagnosis reproducible by eliminating inter- and intra-observer variabilities. In our paper, we describe a computer-aided system for the early diagnosis of melanoma in dermoscopic images. A soft pre-processing phase is performed so as to avoid the loss of details both in texture, colors, and contours, and color-based image segmentation is later carried out using k-means. Features linked to both geometric properties and color characteristics are used to analyze skin lesions through a support vector machine classifier. The PH<sup>2</sup> public database is used for the assessment of the procedure's sensitivity, specificity, and accuracy. A statistical approach is carried out to establish the impact of image quality on performance. The obtained results show remarkable achievements, so our computer-aided approach should be suitable as a Decision Support System for melanoma detection.

**Keywords:** pigmented skin lesion; melanoma; computer-aided detection and diagnosis (CAD); k-means; support vector machine (SVM); skin cancer; dermoscopic image; decision support system (DSS)



**Citation:** Rizzi, M.; Guaragnella, C. A Decision Support System for Melanoma Diagnosis from Dermoscopic Images. *Appl. Sci.* **2022**, *12*, 7007. <https://doi.org/10.3390/app12147007>

Academic Editor: Vangelis Karalis

Received: 6 June 2022

Accepted: 8 July 2022

Published: 11 July 2022

**Publisher's Note:** MDPI stays neutral with regard to jurisdictional claims in published maps and institutional affiliations.



**Copyright:** © 2022 by the authors. Licensee MDPI, Basel, Switzerland. This article is an open access article distributed under the terms and conditions of the Creative Commons Attribution (CC BY) license (<https://creativecommons.org/licenses/by/4.0/>).

## 1. Introduction

Technological progress plays an essential role in the prevention, diagnosis, and treatment of illnesses and diseases and revolutionized healthcare, including patient diagnostic data and patient biological signal facilities and processing [1–4]. Further breakthroughs are expected in various medical areas, particularly in oncology, since cancer is one of the most prevalent causes of death worldwide [5,6]. Technology is projected to play a greater role in medical practice, and the application of computer-aided equipment is especially promising [7–9]. In particular, Computer-Aided Detection (CAD) systems are becoming an important tool in supporting physicians in cancer detection and prevention, particularly when diagnostic images are complex to analyze (due to low quality) and in a high number. The risk of physicians missing subtle abnormalities exists in these situations, especially because images are often low in contrast. In cases of dubious diagnosis, it is common practice for clinicians to behave cautiously and, in order to avoid missing the identification of a malignant case, to prescribe invasive diagnostic procedures, such as biopsies. Inevitably, such a prudent approach results in a high number of negative biopsies with high economic costs.

Melanoma is the most aggressive and deadly form of skin cancer, accounting for about 75% of deaths caused by skin cancer. Its incidence has grown by 15% over the last 10 years compared with the previous decade [10,11]. Early diagnosis is critical and results in a better prognosis. The five-year survival is approximately 98.4% for patients with early stage melanoma compared to just 22.5% for patients with metastatic melanoma [12,13]. Different algorithms have been proposed in the literature for a more objective diagnosis

of skin lesions. They rely on identifying various features, and they classify the lesion's nature according to feature occurrence or non-occurrence [14–16]. Some of them aid decision making by calculating a score (such as the ABCD/ABCDE rule and the seven-point checklist), while others adopt qualitative criteria (such as the Menzies method) [17]. For example, the ABCD algorithm considers the asymmetry of the lesion area, border irregularity, color variegation and diameter, or differential structures of the area under examination. A scoring system has been developed to calculate the total dermoscopy score (TDS) using a linear equation. The TDS allows the grading of lesions and an estimate of their probability of being malignant. A low score means that the lesion is benign ( $TDS < 4.75$ ), a middle score can be interpreted as suspicious ( $4.75 < TDS < 5.45$ ), and a high score means that the lesion is likely to be a malignant melanoma ( $TDS > 5.45$ )

Several non-invasive imaging techniques (such as dermoscopy, confocal scanning laser microscopy, optical coherence tomography, ultrasound, and magnetic resonance) have also been used to support physicians and allow an early diagnosis of malignant skin lesions [18]. These techniques magnify and enhance skin lesions, but early diagnosis by imaging remains quite challenging [19] because there are many different inflammatory skin/lesions and conditions, each with a complex and variable appearance. As the morphology of a skin lesion directly influences the diagnosis, slight morphological differences related to different diseases are difficult to notice without considerable expertise in the specific field. Secondly, simple visual information can lead to misdiagnosis because different pathologies can display similar lesions and because the same lesion can have a different appearance depending on the individual, body part, and stage. Lastly, any diagnosis involving human factors can be difficult to reproduce because of high intra- and inter-observer variability [20,21].

These considerations explain the keen interest in designing CAD systems able to classify pigmented skin lesions and monitor their evolution. These CADs are, obviously, configured as a decision support system (DSS) or as a second opinion for physicians.

The development of CAD systems for the detection and diagnosis of skin lesions is a challenging task since low image contrast, artifacts (such as hairs and bubbles), blood vessels, and depigmented zones often feature in images to be processed. These details can affect the system's performance and reduce its accuracy. Thus, a preprocessing/segmentation phase is usually performed for image quality improvement to extract suitable features that efficiently characterize a lesion's nature. Various studies have shown the lack of an optimal set of features for melanoma detection, and, consequently, researchers have adopted features that they considered to be the most adequate. It is clear that for the optimization of CAD performance and CAD computational efficiency, the adoption of redundant and/or irrelevant features should be avoided.

Although many studies are now available in the literature, skin lesion segmentation and classification can still be improved.

In this paper, the authors propose a new pipeline strategy that adopts computer vision tools for accurate melanoma detection in dermoscopic images. The proposed CAD system uses a color-based k-means procedure for image segmentation and a support vector machine for the classification phase. The attribution of the detected skin lesion to a class of melanoma is driven by extracted features that are based on geometric properties and chromatic characteristics. The PH<sup>2</sup> dataset is adopted as a test-bench, and the reached performance is compared with some popular and recent approaches indicated in the literature [22].

A summary of the most recent classification methods which adopt the PH<sup>2</sup> dataset as a test-bench, is also included in Section 2. Section 3 of our paper deals with the techniques used for the method development. In Section 4, the implemented method is described, and in Section 5 the database adopted for the test of the proposed approach is presented. The achieved performance, discussions, and conclusions complete the paper.

## 2. Related Studies

In recent years, many CAD systems have been developed for the classification of pigmented skin lesions. Some of them have been designed for the detection of global patterns, while others have been used for the detection of localized criteria. The former look for particular patterns of texture structures (pigmented network, globules, etc.), while the latter are based on medical rules, such as ABCDE and the seven-point checklist [23].

None of the various methods in use can be considered optimal as they are as affected by the computational cost, not very high performance, and/or implementation complexity. For this reason, the recognition of skin lesions is still a challenging problem [24]. The challenge is made harder by the low contrast between the lesion and healthy skin, variegated colors, irregular borders, artifacts (such as bubbles or body hairs), and blood vessels [25]. To deal with these issues, in [26], a procedure of feature reduction adopting a higher variance precise entropy is proposed. After a preprocessing phase, a semi-automatic segmentation technique is used, which converts the preprocessed image into the HSV color space and then selects the V-channel as input for both a seeded region growing and a graph cut segmentation. The two segmented images are then fused pixel by pixel, and multilevel feature extraction is performed for lesion classification. Additionally, Banerjee et al. [27] developed a method for melanoma detection based on a combination of a graph theory segmentation technique and L-type fuzzy number-based approximations for a more accurate selection of the cancer area.

The ABCD rule has been used by some [28] to analyze the border and color of skin lesions after the adoption of a Gaussian filter and contour method for the region of interest extraction. Other authors [29] have implemented the adaptive thresholding technique for the segmentation phase and the ABCD scoring method to extract features, which are then classified using a Support Vector Machine. Other studies have approached skin lesions by looking for the presence of patterns. These methods attempt to detect global patterns based on three categories: texture, shape, and color [30]. Luna-Benoso et al. [31] also used texture descriptors based on statistical measurements. Alizadeh et al. [32] converted the image into gray levels and then adopted a local binary pattern and Haralick features as texture features to be extracted from the lesion being tested. A novel approach to extract color and texture features as a single feature—a multi-direction 3D color texture feature—was presented by Warsia et al. [33]. The subsequent detection of melanoma was obtained through a 15 hidden layers backpropagation neural network classifier. It is trained by employing the scaled conjugate gradient backpropagation algorithm.

Moradi et al. [34] adopted a kernel sparse representation for the generation of discriminative sparse codes to represent features in a high-dimensional feature space. They used an adaptive K-Singular Value Decomposition algorithm for learning, segmentation, and classification methods that are undisturbed by image conditions.

The combination of linearly independent and linear prediction algorithms has been used by some authors [35] to measure feature similarity, while in another paper [36], orientation histogram, gradient location, and color features are fused and used to differentiate between malignant and benign skin lesions, adopting a Support Vector Machine classifier.

A deeply supervised encoder–decoder network connected using skip pathways is presented in [37]. This series of skip pathways is composed of convolutional networks and short skip networks. A new convolutional neural network is used for skin lesion segmentation and pixel-wise classification. Additionally, the authors in [38] implemented a convolutional neural network for efficient classification. The network was pre-trained using large AlexNet and ResNet50 transfer learning. Indraswaria et al. [39] adopted MobileNetV2 as the base model for the transfer learning process and added a global pooling layer followed by two fully connected layers as the head model in order to develop a system that could be further implemented on mobile devices.

To discriminate between melanoma and a pathological lesion, the authors in [40] conceived a neural framework in which a low-dimensional but highly discriminative descriptor is derived from local patterns of Gabor-based entropic features. A one-dimensional

vector representation is generated from the extracted Gabor features and then fed into a multilayer neural network for skin lesion classification.

### 3. Adopted Techniques

#### 3.1. K-Means Algorithm

In our proposed system, the segmentation of dermoscopic images is performed using the k-means algorithm, which enables the clustering of the input data into several groups so that elements in the same group have high intra-class similarity while elements belonging to different clusters have low inter-class similarity. In particular, in the unsupervised learning k-means algorithm, each object belongs to only one cluster. The aforementioned method is hence a hard clustering procedure that is part of the region-based segmentation class [41]. This is an iterative procedure that splits the unlabeled data into  $k$  diverse clusters, where  $k$  is a predetermined value. Each cluster is identified by a centroid whose position needs to be conveniently selected considering that the center place affects the achieved result values. Each object of the dataset being tested is associated with the closer centroid. Therefore, the centroid for each cluster is the point that minimizes the sum of distances from all the objects belonging to the cluster.

After the analysis of all the objects composing the dataset, the k-means algorithm computes  $k$  centers, which correspond to the centroids of the  $k$  clusters previously identified. The procedure continues iteratively until the position of the centers does not change.

Denoting with  $X$  and  $M$  the sets of data points and centers, respectively, the k-means aims to minimize the objective function, which is the squared error function defined as:

$$V = \sum_{i=1}^k \sum_{j=1}^{c_i} \|x_j - \mu_i\|^2 \quad (1)$$

where  $c_i$  is the number of data points composing the  $i^{\text{th}}$  cluster,  $k$  is the number of cluster centers, and  $\|x_j - \mu_i\|$  represents the Euclidean distance between the  $i^{\text{th}}$  centroid and the generic data point of the  $i^{\text{th}}$  cluster.

#### 3.2. Support Vector Machine

In machine learning, support vector machines (SVMs) are supervised learning models that analyze data according to the principle of structural risk minimization [42]. They are used for both classification and regression analysis. For classification purposes, SVM tries to find boundaries that separate the different classes of the target variables by maximizing the distance between points closest to the boundaries on either side. The SVM aim is the detection of a hyperplane in a high-dimensional space that distinctly classifies the data points: the procedure finds an optimal hyperplane that classifies new figures based on labeled training data. It is denoted with:

- $x \in \mathbb{R}^n$ —a vector that represents a pattern to be classified;
- $y$ —a scalar that represents the class label;
- $S = \{(x_i, y_i); i = 1, 2, \dots, l\}$ —a given set of  $l$  training examples.

The aim is the implementation of a decision function  $f(x)$  able to classify an input pattern  $x$  that is not necessarily from the training set:

$$f(x) = \sum_{i=1}^l \alpha_i y_i K(x_i, x) + \alpha_0 \quad (2)$$

where  $\alpha_i$  are determined through training, and  $K(.,.)$  is a kernel function. The kernel function transforms data into a higher-dimensional space to make data separation possible. The SVM adoption requires the analysis of three problems: the selection of the kernel function, the detection of the optimal input features subset, and the optimum setting of kernel parameters.

Various hyperplanes could be chosen for the data separation; the SVM algorithm researches a plane with the maximum distance between the data of the classes with the maximum margin.

Training an SVM requires the solution of a very large quadratic programming optimization problem. A simple and widely used method for training an SVM is the Sequential Minimal Optimization (SMO) algorithm. It consists of solving the problem by optimizing the minimal subset, including two elements at each iteration. The advantage of the SMO is that it can be implemented simply and analytically.

#### 4. Implemented CAD System

The aim of the implemented method is the development of a framework able to discriminate melanoma from non-melanoma pigmented skin lesions. The conceived sequential pipeline outlines the way of working of a dermatologist during their clinical routine. For each image, the implemented CAD system firstly identifies the dermoscopic measures and then suggests/hypothesizes a diagnosis to be proposed to the specialist physician for validation. These attributes tend to mimic the ABCD approach. The procedure results assume the role of a second opinion.

The block diagram of the proposed CAD system is shown in Figure 1.

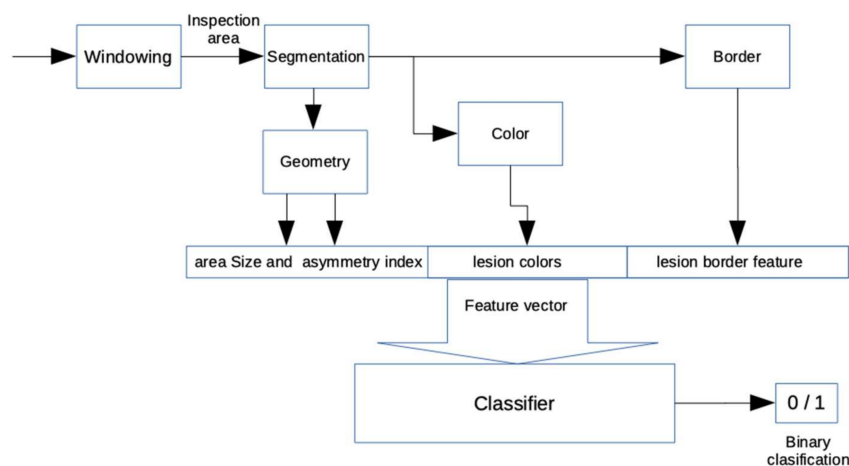


**Figure 1.** Block diagram of the conceived CAD system.

##### 4.1. Windowing and Segmentation Blocks

Preprocessing and segmentation of the region of interest (ROI) is the aim of this block, which is performed by employing the procedure proposed by other authors [35]. The preprocessing phase consists of image windowing: a suitable region having a circular area centered in the center of the image being tested. In this way, color degradation due to wrong/insufficient illumination of the image border is avoided, as shown in Figure 2. This limits the inspection area as, in some cases, the whole region is not included in the ROI.

After the separation of the skin lesion from the rest of the image (ROI localization), the singular value decomposition methodology is adopted for skin lesion image denoising, and then the Red, Green, and Blue (RGB) image being tested is decomposed into a frame of bit-plane layers. By summing the most correlated singular vectors and by using erosion and dilation, an accurate segmentation in coherent areas is obtained.

In Figure 2, the outputs from the implemented steps are shown for a dermoscopic image of a melanoma belonging to the PH<sup>2</sup> database.

##### 4.2. Feature Extraction

###### 4.2.1. Geometry Block

This block considers measures that give information about the lesion shape, which is the size of the lesion area and the asymmetry index.

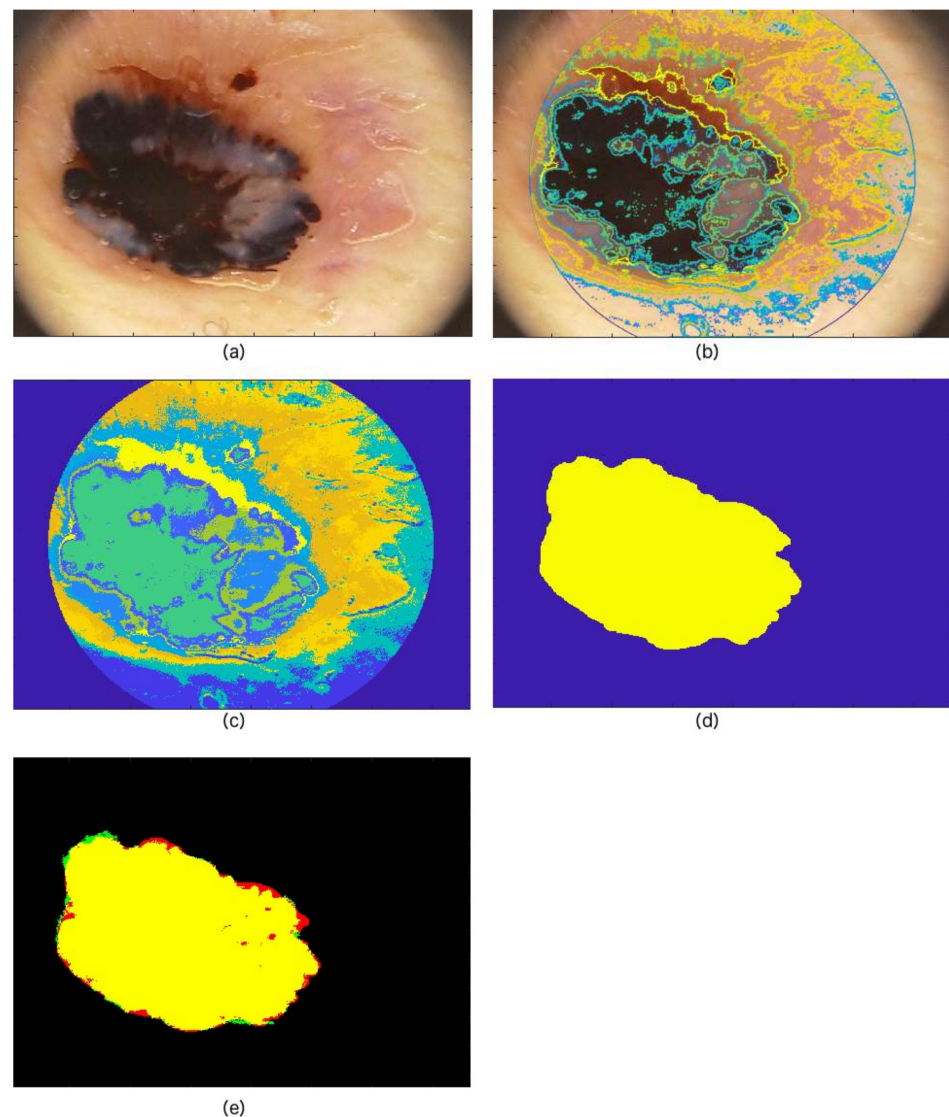


**Figure 2.** Results of the various steps implemented in the segmentation block. (a) Image of the database being tested, (b) ROI localization and detected borders of the coherent color areas, (c) segmentation into coherent color areas, (d) ground-truth provided by the dataset, (e) comparison by overlapping between the ground-true and the obtained segmentation (green: the segmentation performed by the procedure, red: ground-truth, yellow: overlapping area).

A normalized lesion area size is evaluated as the ratio between the sum of the number of pixels composing the segmented lesion and the number of pixels belonging to the ROI.

For the quantification of the asymmetry degree, the segmented lesion area is compared with a circle equivalent to the lesion (same area size), which is centered at the lesion centroid. The circular shape was selected for the intrinsic symmetry of this geometric figure and the invariance with image rotation.

The procedure for the asymmetry index evaluation involves the following steps:

- Computation of the centroid of the segmented skin lesion area;
- Evaluation of the circular area equivalent to the segmented lesion;
- The logical EXOR operation between the equivalent circle and the segmented lesion area (Figure 3).

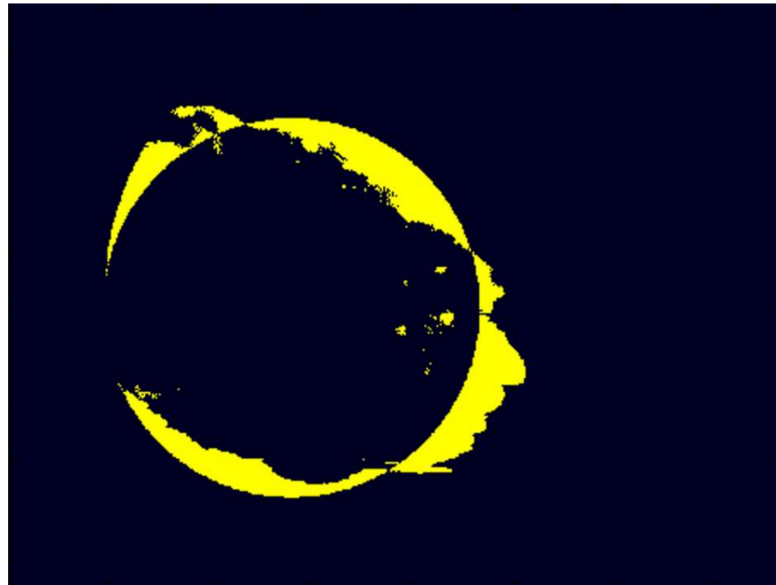


**Figure 3.** Result of the Boolean EXOR operation for the same image of the PH<sup>2</sup> database, previously segmented. The yellow zones are the non-overlapping pixels between the two areas.

The result of this Boolean operation provides information about the skewness of the lesion. The asymmetry degree is evaluated as the ratio of the number of pixels resulting from the EXOR operation to the number of pixels composing the segmented lesion.

#### 4.2.2. Border Detection and Processing

The border detection block extracts the segmented lesion area. The segmented area is used to extract borders that are then chain-coded. Each boundary pixel of the segmented image is represented by a real and an imaginary part so that a sequence of complex numbers is defined to describe the lesion border in relation to the lesion centroid. The real and imaginary part of the detected border is shown in Figure 4, as well as the extracted contour.

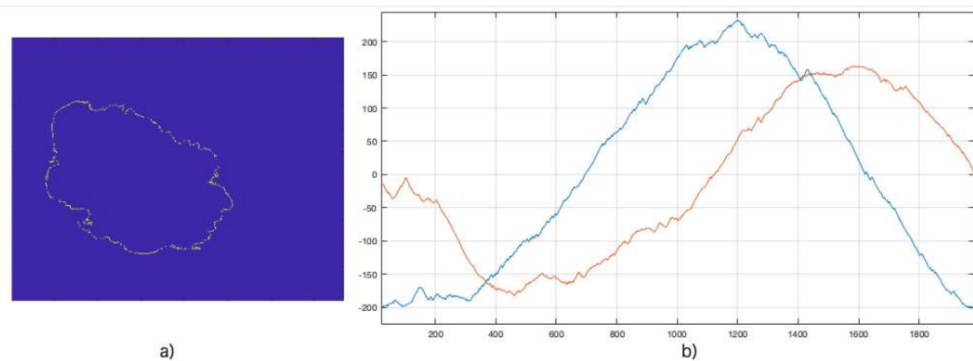


**Figure 4.** (a) Border of the detected lesion area; (b) real (blue line) and imaginary parts (red line) of the complex coding of the border.

To make the border description insensitive to image rotation, the complex data sequence is transformed in the frequency domain via Fast Fourier Transform (FFT). The signal energy computed within a tunable number of bands in the frequency domain is performed to identify the frequency feature to be used in the classification phase.

With  $N$  as the number of the FFT bins to be used and  $M$  intervals in the frequency domain, the feature vector is computed as:

$$E(m) = \sum_{i=0}^{N-M-1} \left\{ \left| X \left[ m \frac{N}{M} + i \right] \right|^2 \right\}, \quad m = 1, 2, \dots, M \quad (3)$$

in which  $E(m)$  represents the energy in each sub-band of contiguous frequency bins in the frequency domain,  $m$  is the index of the  $m^{\text{th}}$  band chosen to describe the feature, and  $X(mN/M + i)$  is the FFT-computed value.

To compare different contour lengths, the FFT is computed on a fixed length by zero-padding and multiplied by a scaling factor, named  $SF$ , defined as the ratio between the chosen FFT length,  $N_{FFT}$ , and the original contour length,  $N_{cont}$ .

$$SF = \frac{N_{FFT}}{N_{cont}} \quad (4)$$

#### 4.2.3. Color Block

The aim of the block in question is the definition of a palette of colors composing the segmented lesion area to be used as a color feature for lesion classification. For this purpose, a lesion segmentation is carried out in coherent color areas by a  $k$ -means algorithm with an  $N_c$  number of areas, where  $N_c$  is a tunable integer positive. The implemented CAD system provides physicians with the option of viewing these color areas, which may help in assessing the lesion scoring.

In each color-based segmented area using  $k$ -means, the color mean value is evaluated considering the color components of the RGB image being tested. For each image of the database, a palette of  $N_c$  different colors is obtained.

To compare palettes of different skin lesion images, a color transformation from RGB to Hue, Saturation, and Value (HSV) is implemented, and only the  $H$  and  $S$  components are retained, as the  $V$  component is illumination-dependent, while  $H$  and  $S$  components define the tint. With this approach, a color space is selected that has a relation with human perception and characterizes the color model like the human mind [36].

To compare different palettes corresponding to different lesions within a classification system, a sorting mechanism is required. To this aim, a complex number is defined, which is expressed as:

$$X_n = H_n + j S_n \text{ for } 1 \leq n \leq N_c \quad (5)$$

where  $H_n$  and  $S_n$  are the hue and saturation values of the  $n^{\text{th}}$  detected color.

For each ROI, a color-based feature vector is created (named palette) that contains the  $X_n$  numbers, sorted in ascending order of  $\arg(X_n)$ , denoting with  $\arg(X_n)$  the argument of  $X_n$ . In Figure 5, the color palette of the image previously segmented is shown.

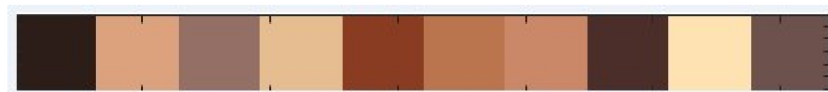


**Figure 5.** An example of a color palette extracted by the image.

Changes in pigment inside a skin lesion are important details for an accurate classification; hence, each pixel of the color-based segmented areas is analyzed, and the difference between the pixel color and the mean color value of the segmented area to which that pixel belongs is measured. The color difference between the lesion area and the mean color of each segmented area obtained by the  $k$ -means procedure is evaluated to compose the difference image, known as dyschromia. The image corresponding to the difference previously considered is shown in Figure 6a. Such an image, magnified by a tunable parameter, is submitted to clinicians as accompanying information about the local color variation. The implemented procedure provides the option of analyzing the dyschromia image if deemed appropriate. The image obtained by substituting the mean color in each area, named the “flattened image”, is shown in Figure 6b.

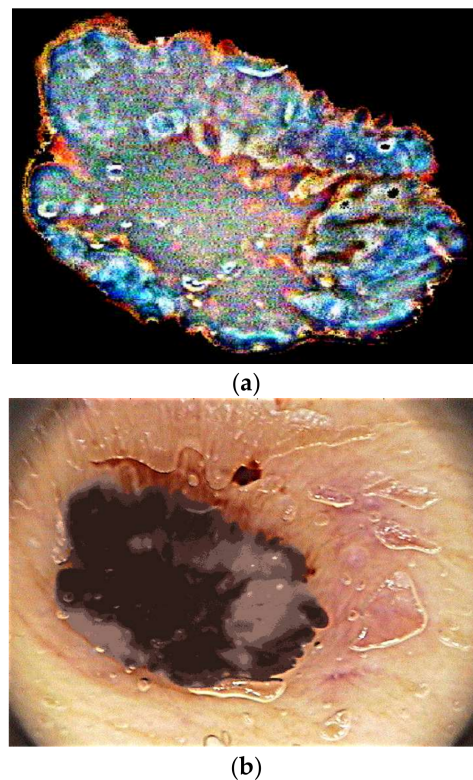


**Figure 6.** (a) Dyschromia image obtained considering the image segmented in coherent color areas. (b) Corresponding flattened image.

#### 4.3. Classification Block

The aim of the classification block is the diagnosis of previously detected and localized skin lesions. Binary classification is used: melanoma and non-melanoma nevi. Each skin lesion being tested is represented by its own features (feature set), which are the classifier inputs. The output is the class to which the lesion belongs, namely, the melanoma class or the non-melanoma class. The feature to be used in the classification phase is composed of several parameters, namely:

- Area size–feature size = 1.
- Symmetry Index–feature size = 1.
- [R, G, B]–feature size =  $3 \times N_c$ .
- Border–feature size = a vector of energies in the  $N_{FFT}$  sub-bands.

A feature set composed of  $(2 + 3 \times N_c + N_{FFT})$  elements is obtained for each image of the database considering the whole of the evaluated features.

The SVM technique is used, and the logistic function is adopted as a kernel. The five-folded cross-validation method is implemented for the tuning of kernel parameters.

### 5. Database Used for CAD System Validation

The publicly available PH<sup>2</sup> database is the dataset used as a test-bench for the method validation [22]. A total of 200 dermoscopic images divided into 80 atypical nevi, 80 common nevi, and 40 melanomas formed the dataset being tested. Images were 8-bit RGB with a  $768 \times 560$  pixel resolution captured by a lens with a  $2\times$  magnification.

The PH<sup>2</sup> database includes manual segmentation, clinical and histological diagnosis of the skin lesion, as well as other important dermoscopic criteria, such as the assessment of the lesion asymmetry, and the identification of colors, pigment network, dots, globules, streaks, regression areas, and the blue-whitish veil. All the included dermoscopic images are from skin type II or III according to the Fitzpatrick skin type classification. Accordingly, skin colors in the PH<sup>2</sup> database range from white to cream white. The manual segmentation

of skin lesions is provided by expert dermatologists and is available as a binary mask in which pixels with an intensity value of 1 correspond to the segmented lesion, while pixels with a value of 0 correspond to the background. For each image, the following information is included:

- A ground truth binary image, manually generated by expert dermatologists, containing the skin lesion area.
- Clinical and histological diagnosis.
- Dermoscopic criteria.

All the dermoscopic criteria indicated in the database take into account most of the features that need to be considered during diagnosis procedures, such as the ABCD rule, the seven-point checklist, and the Menzies method.

## 6. Performance Evaluation

### 6.1. Evaluation Metrics

Therefore, to evaluate and measure the effectiveness of the implemented CAD system in classifying a dermoscopic image of skin lesions, some of the performance measurement metrics indicated in the International Skin Imaging Collaboration (ISIC) challenge were considered. Accuracy, sensitivity, specificity, and precision were assessed by adopting the following expressions:

$$\text{Sensitivity (Se)} = \frac{TP}{TP + FN} \quad (6)$$

$$\text{Specificity (Sp)} = \frac{TN}{TN + FP} \quad (7)$$

$$\text{Precision (Pr)} = \frac{TP}{TP + FP} \quad (8)$$

$$\text{Accuracy (AC)} = \frac{TP + TN}{TP + FP + TN + FN} \quad (9)$$

$$\text{F1 score} = \frac{2TP}{2TP + FP + FN} \quad (10)$$

in which:

- $TP$  (true positives) is the number of melanomas correctly classified inside the database.
- $FN$  (false negatives) is the number of melanomas that the algorithm is not able to correctly classify and, consequently, considers non-melanomas.
- $FP$  (false positives) is the number of non-melanomas that the algorithm is not able to correctly classify and, consequently, considers melanomas.
- $TN$  (true negatives) is the number of non-melanomas correctly classified inside the database.

According to the intended use of the developed CAD system, some of the measures above mentioned play a role of relative significance and impact; hence, they are prioritized: for example, sensitivity is considered to be relevant if the failure to detect the disease can have serious health and survival consequences, such as in treatable malignancies [43,44]. Broadly speaking, a trade-off between the various measures is inevitable based on the impact of FP and FN diagnoses and on disease prevalence [45,46]

### 6.2. Achieved Results

For the performance evaluation of the implemented CAD system,  $N_c = 10$  and  $N_{FFT} = L/50$ , where  $L$  is the length used for the FFT to consider the same frequency bins in the definition of the contour feature.  $L = 10,000$  is selected in the performed study.

To quantify the method's efficiency and validity, a publicly available PH<sup>2</sup> database of skin lesion dermoscopic images is used. Thereby, a comparative analysis with some recent decision support systems for melanoma diagnosis indicated in literature is possible. The designed diagnostic framework shows competitive performance, with Se, Sp, Ac, Pr, and F1

scores of 97.8%, 99.14%, 98%, 99.1%, and 98.1%, respectively. In Table 1, the implemented method results are presented and compared with some popular procedures published in the last three years.

**Table 1.** Performance comparison among some most recent procedures indicated in literature that used the PH<sup>2</sup> database.

Technique	Se (%)	Sp (%)	Ac (%)
SVM [26]	97.90	-	98.20
YOLO [27]	97.5	97.5	97.5
TDS index [28]	60.5	89.5	84
SVM [29]	100	87.5	92.5
Dynamic selection [30]	97	100	97
Associative model [31]	94.4	98.7	97.8
MobileNet/DenseNet [32]	100	96.88	97.5
Neural Network [33]	98.1	92.5	97
Kernel sparse coding scheme [34]	100	91.98	93.50
SVM [35]	92.50	91.30	91.90
DCNN [37]	93	95	95
ANN/CNN [38]	98.30	96.72	97.50
MobileNetV2 [39]	33	92	72
Multilevel Neural Network [40]	100	96.87	97.5
SVM (Proposed method)	97.8	99.14	98

## 7. Discussions

Researchers have been keen to develop an efficient and high-performing CAD for medical use. Lower computation cost, real-time processing, and open architecture are also welcome characteristics.

The choice of the database used as a test-bench is crucial, as the performance achieved by a procedure usually depends on it. The PH2 database adopted by the authors provides a challenging bench-test because some of its images are dimly lit, contain hairs, are connected to the boundary edge of the provided image, or occupy almost the entire image area.

In several studies in the literature, some of the images from the PH2 database have been discarded without providing a detailed description of image-selection criteria [47–51]. The results reported in these papers are consequently difficult to verify, their method cannot be reproduced, and performance comparisons with other studies are difficult. We are of the opinion that the number of images used and/or discarded should always be reported.

Image quality in the chosen database is inconsistent; hence, a subset of low-quality images has been identified to assess the impact of image quality on the performance of CAD systems. Denoting by ND the number of poor-quality images to be discarded from the dataset ( $0 \leq ND \leq 49$ ), a statistic of the method performance with regard to low-quality images is extracted. The study is carried out varying ND within the previously defined range, and a statistic of the performance measurement metrics is accumulated for every ND. For each value of the ND parameter, the approach is repeated randomly, changing the selected low-quality images over thousands of different choices. For the sake of comparison, precision and specificity are considered performance metrics.

To simply compare the results obtained with different selections of the images to be discarded, the k-means technique is used with  $k = 2$ .

In Figure 7, the boxplot of the performance achieved with ND equal to 20 is shown.

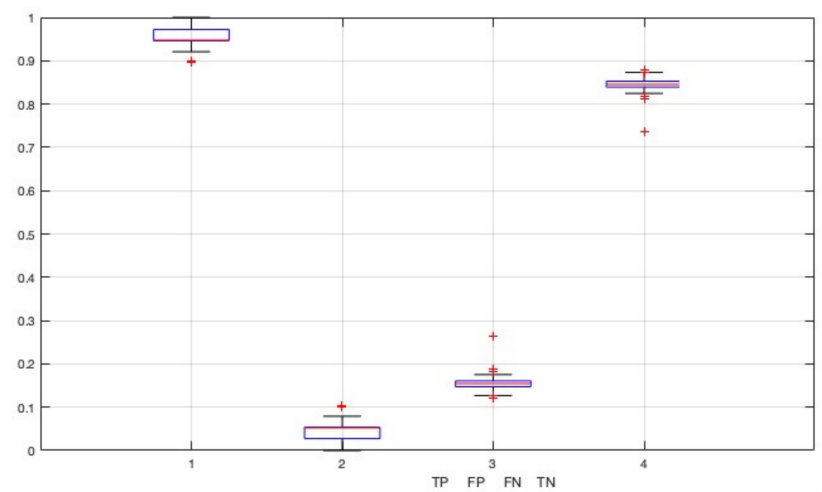


**Figure 7.** The box plots of *TN*, *TP*, *FN*, and *FP* statistics for PH2 database with  $ND = 20$ .

In Figure 8, the boxplot of the obtained performance is plotted for a given number of discarded low-quality images. It is clear that even after discarding just a few images, the system performance changes significantly, and high performance can be obtained with a selective choice of images.

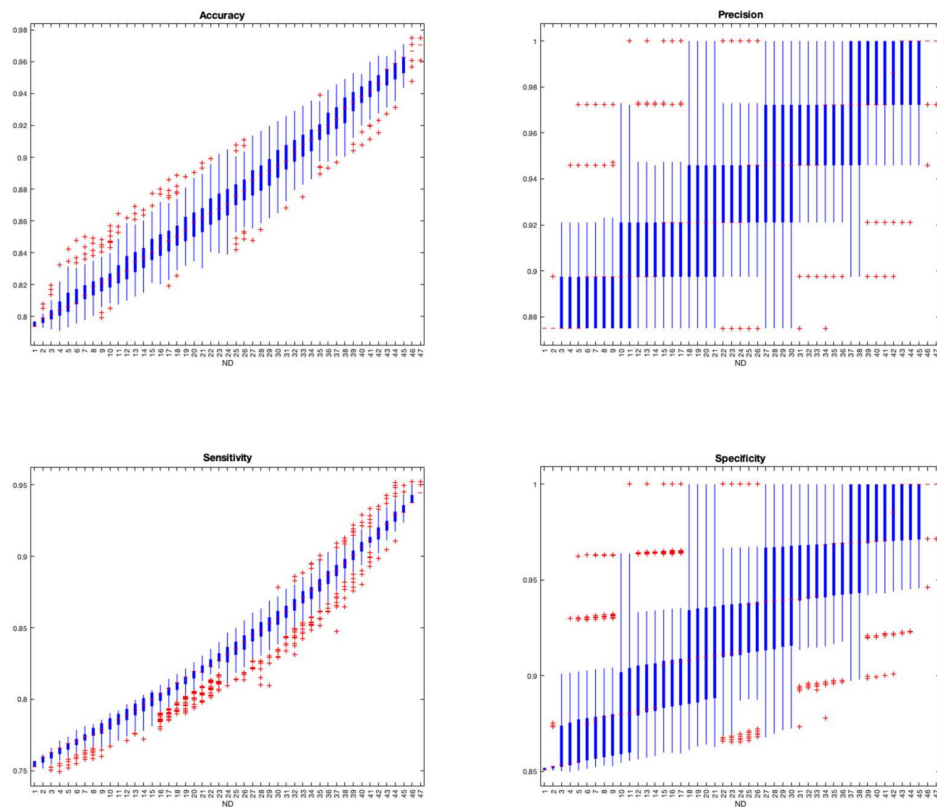


**Figure 8.** Performance of the CAD system for different  $ND$  values.

Figure 8 highlights the great impact of image quality on CAD performance. Therefore, care should be taken in the construction of the database during the image acquisition phase, requiring optimal focusing, good and fixed contrast, and avoiding reflections and color changes as a consequence of different color temperatures of light used in the acquisition phase.

## 8. Conclusions

The increasing incidence of melanoma worldwide, the clear advantages of early diagnosis, and the difficulties of accessing expert dermatologic services in remote areas underpin the importance of the researcher's endeavors in developing decision support systems less dependent on human expertise.

Several requirements have to be fulfilled by a CAD system before it can be safely adopted in clinical practice, such as improvement in specialist performance, perfect integration into the workflow, and time savings in diagnosis.

This paper proposes the development of a CAD system for pigmented skin lesion diagnosis. Our method is inspired by clinical practice but characterizes the criteria for melanoma detection in a custom way through original features linked to parameters routinely used by physicians. After the localization of the region of interest, the conceived pipeline framework characterizes the lesion being tested through features linked to both geometric properties and chromatic characteristics. A data-driven approach is selected for the classification phase, and the diagnosis is performed by defining a binary decision system that divides lesions into melanoma and non-melanoma categories.

The proposed method is very versatile. It is an open architecture where each block is an object-oriented module and can be upgraded individually to improve the CAD system performance.

**Author Contributions:** Conceptualization, C.G. and M.R.; methodology, C.G. and M.R.; software, C.G.; validation, C.G. and M.R.; formal analysis, C.G. and M.R.; investigation, M.R. and C.G.; resources, C.G. and M.R.; data curation, M.R.; writing—original draft preparation, M.R.; writing—review and editing, C.G. and M.R.; visualization, C.G.; supervision, C.G. and M.R. All authors have read and agreed to the published version of the manuscript.

**Funding:** This research received no external funding.

**Institutional Review Board Statement:** Not applicable.

**Informed Consent Statement:** Not applicable.

**Conflicts of Interest:** The authors declare no conflict of interest.

## References

1. Kraus, S.; Schiavone, F.; Pluzhnikova, A.; Invernizzi, A.C. Digital transformation in healthcare: Analyzing the current state-of-research. *J. Bus. Res.* **2021**, *123*, 557–567. [CrossRef]
2. Guaragnella, C.; Rizzi, M.; Giorgio, A. Marginal Component Analysis of ECG Signals for Beat-to-Beat Detection of Ventricular Late Potentials. *Electronics* **2019**, *8*, 1000. [CrossRef]
3. Ghoniem, R.M. A Novel Bio-Inspired Deep Learning Approach for Liver Cancer Diagnosis. *Information* **2020**, *11*, 80. [CrossRef]
4. Rizzi, M.; D'Aloia, M.; Longo, A. Digital watermarking for healthcare: A survey of ECG watermarking methods in telemedicine. *Int. J. Comput. Sci. Eng.* **2020**, *23*, 235–249. [CrossRef]
5. He, Y.; Li, W.; Zhang, W.; Zhang, S.; Pi, X.; Liu, H. Research on Segmentation and Classification of Heart Sound Signals Based on Deep Learning. *Appl. Sci.* **2021**, *11*, 651. [CrossRef]
6. Rizzi, M.; D'Aloia, M.; Castagnolo, B. A fully automatic system for detection of breast microcalcification clusters. *J. Med. Biol. Eng.* **2010**, *30*, 181–188.
7. Giorgio, A.; Rizzi, M.; Guaragnella, C. Efficient Detection of Ventricular Late Potentials on ECG Signals Based on Wavelet Denoising and SVM Classification. *Information* **2019**, *10*, 328. [CrossRef]
8. Song, W. A New Method for Refined Recognition for Heart Disease Diagnosis Based on Deep Learning. *Information* **2020**, *11*, 556. [CrossRef]
9. Rizzi, M.; D'Aloia, M.; Castagnolo, B. Semiconductor Detectors and Principles of Radiation-matter Interaction. *J. Appl. Sci.* **2010**, *10*, 3141–3155. [CrossRef]
10. Melanoma. Available online: <https://www.epicentro.iss.it/melanoma/> (accessed on 15 March 2022).
11. Melanoma: Incidenza e Mortalità. Available online: <https://www.infomedics.it/therapeutic-areas/melanoma.html> (accessed on 15 March 2022).
12. Melanoma Survival Rates. Available online: <https://www.curemelanoma.org/about-melanoma/melanoma-staging/melanoma-survival-rates/> (accessed on 15 March 2022).
13. Blundo, A.; Cignoni, A.; Banfi, T.; Ciuti, G. Comparative Analysis of Diagnostic Techniques for Melanoma Detection: A Systematic Review of Diagnostic Test Accuracy Studies and Meta-Analysis. *Front. Med.* **2021**, *8*, 637069. [CrossRef]

14. Guaragnella, C.; Rizzi, M. Simple and Accurate Border Detection Algorithm for Melanoma Computer Aided Diagnosis. *Diagnostics* **2020**, *10*, 423. [[CrossRef](#)]
15. Khana, M.A.; Sharif, M.; Akramd, T.; Bukhari, S.A.C.; Nayak, R.S. Developed Newton-Raphson based deep features selection framework for skin lesion recognition. *Pattern Recognit. Lett.* **2020**, *129*, 293–303. [[CrossRef](#)]
16. Rizzi, M.; D'Aloia, M.; Cice, G. Computer aided evaluation (CAE) of morphologic changes in pigmented skin lesions. In *Lecture Notes in Computer Science (including subseries Lecture Notes in Artificial Intelligence and Lecture Notes in Bioinformatics), Processing of the New Trends in Image Analysis and Processing—ICIAP 2015, Genoa, Italy, 7–8 September 2015*; Springer: Cham, Switzerland, 2015; Volume 9281, pp. 250–257. [[CrossRef](#)]
17. Johr, R.H. Dermoscopy: Alternative melanocytic algorithms—the ABCD rule of dermatoscopy, Menzies scoring method, and 7-point checklist. *Clin. Dermatol.* **2002**, *20*, 240–247. [[CrossRef](#)]
18. Popescu, D.; El-Khatib, M.; El-Khatib, H.; Ichim, L. New Trends in Melanoma Detection Using Neural Networks: A Systematic Review. *Sensors* **2022**, *22*, 496. [[CrossRef](#)]
19. Zhang, B.; Zhou, X.; Hao, L.; Zhang, H.; Yang, H.; Ma, J.; Ma, L. Opportunities and Challenges: Classification of Skin Disease Based on Deep Learning. *Chin. J. Mech. Eng.* **2021**, *34*, 112. [[CrossRef](#)]
20. Rizzi, M.; D'Aloia, M. Computer aided system for breast cancer diagnosis. *Biomed. Eng. Appl. Basis Commun.* **2014**, *26*, 3–11. [[CrossRef](#)]
21. Soudani, A.; Barhoumi, W. An image-based segmentation recommender using crowdsourcing and transfer learning for skin lesion extraction. *Expert Syst. Appl.* **2019**, *118*, 400–410. [[CrossRef](#)]
22. Mendonc, T.; Ferreira, M.P.; Marques, J.S.; Marcal, A.R.S. PH 2-A dermoscopic image database for research and benchmarking. In *Proceedings of the 2013 35th Annual International Conference of the IEEE Engineering in Medicine and Biology Society (EMBC), Osaka, Japan, 3–7 July 2013*; pp. 5437–5440.
23. Barata, C.; Celebi, M.E.; Marques, J.S. Development of a clinically oriented system for melanoma diagnosis. *Pattern Recognit.* **2017**, *69*, 270–285. [[CrossRef](#)]
24. Singh, L.; Janghel, R.R.; Sahu, S.P. Automated CAD System for Skin Lesion Diagnosis: A Review. In *Advances in Biomedical Engineering and Technology; Lecture Notes in Bioengineering; Rizvanov, A.A., Singh, B.K., Ganasala, P., Eds.; Springer: Singapore, 2021*; pp. 295–320. [[CrossRef](#)]
25. Rizzi, M.; Guaragnella, C. Skin Lesion segmentation using Image Bit Plane Multilayer approach. *Appl. Sci.* **2020**, *10*, 3045. [[CrossRef](#)]
26. Rehman, A.; Khan, M.A.; Mehmood, Z.; Saba, T.; Sardaraz, M.; Rashid, M. Microscopic melanoma detection and classification: A framework of pixel-based fusion and multilevel features reduction. *Microsc. Res. Tech.* **2020**, *83*, 410–423. [[CrossRef](#)]
27. Banerjee, S.; Singh, S.K.; Chakraborty, A.; Das, A.; Bag, R. Melanoma Diagnosis Using Deep Learning and Fuzzy Logic. *Diagnostics* **2020**, *10*, 577. [[CrossRef](#)]
28. Senan, E.M.; Jadhav, M.E. Analysis of dermoscopy images by using ABCD rule for early detection of skin cancer. *Glob. Transit. Proc.* **2021**, *2*, 1–7. [[CrossRef](#)]
29. Singh, L.; Janghel, R.R.; Sahu, S.P. Designing a Retrieval-Based Diagnostic Aid using Effective Features to Classify Skin Lesion in Dermoscopic Images. *Procedia Comput. Sci.* **2020**, *167*, 2172–2180. [[CrossRef](#)]
30. Pathana, S.; Prabhub, K.G.; Siddalingaswamy, P.C. Automated detection of melanocytes related pigmented skin lesions: A clinical framework. *Biomed. Signal Process. Control* **2019**, *51*, 59–72. [[CrossRef](#)]
31. Luna-Benoso, B.; Martínez-Perales, J.C.; Cortés-Galicia, J.; Flores-Carapia, R.; Silva-García, V.M. Melanoma Detection in Dermoscopic Images Using a Cellular Automata Classifier. *Computers* **2022**, *11*, 8. [[CrossRef](#)]
32. Alizadeh, S.M.; Mahloojifar, A. Automatic skin cancer detection in dermoscopy images by combining convolutional neural networks and texture features. *Int. J. Imaging Syst. Technol.* **2021**, *31*, 695–707. [[CrossRef](#)]
33. Warsia, F.; Khanama, R.; Kamyab, S.; Suárez-Arauj, C.P. An efficient 3D color-texture feature and neural network technique for melanoma detection. *Inform. Med. Unlocked* **2019**, *17*, 100176. [[CrossRef](#)]
34. Moradi, N.; Mahdavi-Amiri, N. Kernel sparse representation based model for skin lesions segmentation and classification. *Comput. Methods Programs Biomed.* **2019**, *182*, 105038. [[CrossRef](#)] [[PubMed](#)]
35. Hu, K.; Niu, X.; Liu, S.; Zhang, Y.; Cao, C.; Xiao, F.; Yang, W.; Gao, X. Classification of melanoma based on feature similarity measurement for codebook learning in the bag-of-features model. *Biomed. Signal Process. Control* **2019**, *51*, 200–209. [[CrossRef](#)]
36. Upadhyay, P.K.; Chandra, S. An improved bag of dense features for skin lesion recognition. *J. King Saud Univ.-Comput. Inf. Sci.* **2022**, *34*, 520–525. [[CrossRef](#)]
37. Adegun, A.A.; Viriri, S. Deep Learning-Based System for Automatic Melanoma Detection. *IEEE Access* **2020**, *8*, 7160–7172. [[CrossRef](#)]
38. Alsaade, F.W.; Aldhyani, T.H.H.; Al-Adhaileh, M.H. Developing a Recognition System for Diagnosing Melanoma Skin Lesions Using Artificial Intelligence Algorithms. *Comput. Math. Methods Med.* **2021**, *2021*, 9998379. [[CrossRef](#)] [[PubMed](#)]
39. Indraswaria, R.; Rokhanab, R.; Herulambang, W. Melanoma image classification based on MobileNetV2 network. *Procedia Comput. Sci.* **2022**, *197*, 198–207. [[CrossRef](#)]
40. Bakheet, S.; Al-Hamadi, A. Computer-Aided Diagnosis of Malignant Melanoma Using Gabor-Based Entropic Features and Multilevel Neural Networks. *Diagnostics* **2020**, *10*, 822. [[CrossRef](#)]

41. Debelee, T.G.; Schwenker, F.; Rahimeto, S.; Yohannes, D. Evaluation of modified adaptive k-means segmentation algorithm. *Comput. Vis. Media* **2019**, *5*, 347–361. [[CrossRef](#)]
42. Rizzi, M.; D'aloia, M.; Castagnolo, B. A supervised method for microcalcification cluster diagnosis. *Integr. Comput.-Aided Eng.* **2013**, *20*, 157–167. [[CrossRef](#)]
43. Giorgio, A.; Guaragnella, C.; Rizzi, M. An Effective CAD System for Heart Sound Abnormality Detection. *Circuits Syst. Signal Process.* **2022**, *41*, 2845–2870. [[CrossRef](#)]
44. D'Aloia, M.; Longo, A.; Russo, R.; Stanisci, S.; Amendolare, D.; Rizzi, M.; Vessia, M.; Lomastro, F. An innovative LPWA network scheme to increase system reliability in remote monitoring. In Proceedings of the 2017 IEEE Workshop on Environmental, Energy and Structural Monitoring Systems, Milan, Italy, 24–25 July 2017; pp. 1–6. [[CrossRef](#)]
45. Chubak, J.; Pocobelli, G.; Weiss, N.S. Tradeoffs between accuracy measures for electronic health care data algorithms. *J. Clin. Epidemiol.* **2012**, *65*, 343–349.e2. [[CrossRef](#)]
46. Trevethan, R. Sensitivity, Specificity, and Predictive Values: Foundations, Plabilities, and Pitfalls in Research and Practice. *Front. Public Health* **2017**, *5*, 307. [[CrossRef](#)]
47. Ma, Z.; Tavares, J.M.R.S. A novel approach to segment skin lesions in dermoscopic images based on a deformable model. *IEEE J. Biomed. Health Inform.* **2016**, *20*, 615–623. [[CrossRef](#)]
48. Yang, T.; Chen, Y.; Lu, J.; Fan, Z. Sampling with level set for pigmented skin lesion segmentation. *Signal Image Video Process.* **2019**, *13*, 813–821. [[CrossRef](#)]
49. Ünver, H.M.; Ayan, E. Skin Lesion Segmentation in Dermoscopic Images with Combination of YOLO and GrabCut Algorithm. *Diagnostics* **2019**, *9*, 72. [[CrossRef](#)] [[PubMed](#)]
50. Ahn, E.; Kim, J.; Bi, L.; Kumar, A.; Li, C.; Fulham, M.; Feng, D.D. Saliency-Based Lesion Segmentation Via Background Detection in Dermoscopic Images. *IEEE J. Biomed. Health Inform.* **2017**, *21*, 1685–1693. [[CrossRef](#)] [[PubMed](#)]
51. Bi, L.; Kim, J.; Ahn, E.; Feng, D.; Fulham, M. Automated skin lesion segmentation via image-wise supervised learning and multi-scale superpixel based cellular automata. In Proceedings of the 2016 IEEE 13th International Symposium on Biomedical Imaging (ISBI 2016), Prague, Czech Republic, 13–16 April 2016; pp. 1059–1062. [[CrossRef](#)]